Measurement of the inclusive-isolated prompt-photon cross section in $p\bar{p}$ collisions using the full CDF data set

T. Aaltonen,[21] M.G. Albrow,[15] S. Amerio[ll],[39] D. Amidei,[31] A. Anastassov[w],[15] A. Annovi,[17] J. Antos,[12] G. Apollinari,[15] J.A. Appel,[15] T. Arisawa,[51] A. Artikov,[13] J. Asaadi,[47] W. Ashmanskas,[15] B. Auerbach,[2] A. Aurisano,[47] F. Azfar,[38] W. Badgett,[15] T. Bae,[25] A. Barbaro-Galtieri,[26] V.E. Barnes,[43] B.A. Barnett,[23] P. Barria[nn],[41] P. Bartos,[12] M. Bauce[ll],[39] F. Bedeschi,[41] S. Behari,[15] G. Bellettini[mm],[41] J. Bellinger,[53] D. Benjamin,[14] A. Beretvas,[15] A. Bhatti,[45] K.R. Bland,[5] B. Blumenfeld,[23] A. Bocci,[14] A. Bodek,[44] D. Bortoletto,[43] J. Boudreau,[42] A. Boveia,[11] L. Brigliadori[kk],[6] C. Bromberg,[32] E. Brucken,[21] J. Budagov,[13] H.S. Budd,[44] K. Burkett,[15] G. Busetto[ll],[39] P. Bussey,[19] P. Butti[mm],[41] A. Buzatu,[19] A. Calamba,[10] S. Camarda,[4] M. Campanelli,[28] F. Canelli[ee],[11] B. Carls,[22] D. Carlsmith,[53] R. Carosi,[41] S. Carrillo[l],[16] B. Casal[j],[9] M. Casarsa,[48] A. Castro[kk],[6] P. Catastini,[20] D. Cauz[sstt],[48] V. Cavaliere,[22] A. Cerri[e],[26] L. Cerrito[r],[28] Y.C. Chen,[1] M. Chertok,[7] G. Chiarelli,[41] G. Chlachidze,[15] K. Cho,[25] D. Chokheli,[13] A. Clark,[18] C. Clarke,[52] M.E. Convery,[15] J. Conway,[7] M. Corbo[z],[15] M. Cordelli,[17] C.A. Cox,[7] D.J. Cox,[7] M. Cremonesi,[41] D. Cruz,[47] J. Cuevas[y],[9] R. Culbertson,[15] N. d'Ascenzo[v],[15] M. Datta[hh],[15] P. de Barbaro,[44] L. Demortier,[45] M. Deninno,[6] M. D'Errico[ll],[39] F. Devoto,[21] A. Di Canto[mm],[41] B. Di Ruzza[p],[15] J.R. Dittmann,[5] S. Donati[mm],[41] M. D'Onofrio,[27] M. Dorigo[uu],[48] A. Driutti[sstt],[48] K. Ebina,[51] R. Edgar,[31] R. Erbacher,[7] S. Errede,[22] B. Esham,[22] S. Farrington,[38] J.P. Fernández Ramos,[29] R. Field,[16] G. Flanagan[t],[15] R. Forrest,[7] M. Franklin,[20] J.C. Freeman,[15] H. Frisch,[11] Y. Funakoshi,[51] C. Galloni[mm],[41] A.F. Garfinkel,[43] P. Garosi[nn],[41] H. Gerberich,[22] E. Gerchtein,[15] S. Giagu,[46] V. Giakoumopoulou,[3] K. Gibson,[42] C.M. Ginsburg,[15] N. Giokaris,[3,*] P. Giromini,[17] V. Glagolev,[13] D. Glenzinski,[15] M. Gold,[34] D. Goldin,[47] A. Golossanov,[15] G. Gomez,[9] G. Gomez-Ceballos,[30] M. Goncharov,[30] O. González López,[29] I. Gorelov,[34] A.T. Goshaw,[14] K. Goulianos,[45] E. Gramellini,[6] C. Grosso-Pilcher,[11] J. Guimaraes da Costa,[20] S.R. Hahn,[15] J.Y. Han,[44] F. Happacher,[17] K. Hara,[49] M. Hare,[50] R.F. Harr,[52] T. Harrington-Taber[m],[15] K. Hatakeyama,[5] C. Hays,[38] J. Heinrich,[40] M. Herndon,[53] A. Hocker,[15] Z. Hong,[47] W. Hopkins[f],[15] S. Hou,[1] R.E. Hughes,[35] U. Husemann,[54] M. Hussein[cc],[32] J. Huston,[32] G. Introzzi[ppqq],[41] M. Iori[rr],[46] A. Ivanov[o],[7] E. James,[15] D. Jang,[10] B. Jayatilaka,[15] E.J. Jeon,[25] S. Jindariani,[15] M. Jones,[43] K.K. Joo,[25] S.Y. Jun,[10] T.R. Junk,[15] M. Kambeitz,[24] T. Kamon,[25,47] P.E. Karchin,[52] A. Kasmi,[5] Y. Kato[n],[37] W. Ketchum[ii],[11] J. Keung,[40] B. Kilminster[ee],[15] D.H. Kim,[25] H.S. Kim[bb],[15] J.E. Kim,[25] M.J. Kim,[17] S.H. Kim,[49] S.B. Kim,[25] Y.J. Kim,[25] Y.K. Kim,[11] N. Kimura,[51] M. Kirby,[15] K. Kondo,[51,*] D.J. Kong,[25] J. Konigsberg,[16] A.V. Kotwal,[14] M. Kreps,[24] J. Kroll,[40] M. Kruse,[14] T. Kuhr,[24] M. Kurata,[49] A.T. Laasanen,[43] S. Lammel,[15] M. Lancaster,[28] K. Lannon[x],[35] G. Latino[nn],[41] H.S. Lee,[25] J.S. Lee,[25] S. Leo,[22] S. Leone,[41] J.D. Lewis,[15] A. Limosani[s],[14] E. Lipeles,[40] A. Lister[a],[18] Q. Liu,[43] T. Liu,[15] S. Lockwitz,[54] A. Loginov,[54] D. Lucchesi[ll],[39] A. Lucà,[17,15] J. Lueck,[24] P. Lujan,[26] P. Lukens,[15] G. Lungu,[45] J. Lys,[26,*] R. Lysak[d],[12] R. Madrak,[15] P. Maestro[nn],[41] S. Malik,[45] G. Manca[b],[27] A. Manousakis-Katsikakis,[3] L. Marchese[jj],[6] F. Margaroli,[46] P. Marino[oo],[41] K. Matera,[22] M.E. Mattson,[52] A. Mazzacane,[15] P. Mazzanti,[6] R. McNulty[i],[27] A. Mehta,[27] P. Mehtala,[21] C. Mesropian,[45] T. Miao,[15] D. Mietlicki,[31] A. Mitra,[1] H. Miyake,[49] S. Moed,[15] N. Moggi,[6] C.S. Moon[z],[15] R. Moore[ffgg],[15] M.J. Morello[oo],[41] A. Mukherjee,[15] Th. Muller,[24] P. Murat,[15] M. Mussini[kk],[6] J. Nachtman[m],[15] Y. Nagai,[49] J. Naganoma,[51] I. Nakano,[36] A. Napier,[50] J. Nett,[47] T. Nigmanov,[42] L. Nodulman,[2] S.Y. Noh,[25] O. Norniella,[22] L. Oakes,[38] S.H. Oh,[14] Y.D. Oh,[25] T. Okusawa,[37] R. Orava,[21] L. Ortolan,[4] C. Pagliarone,[48] E. Palencia[e],[9] P. Palni,[34] V. Papadimitriou,[15] W. Parker,[53] G. Pauletta[sstt],[48] M. Paulini,[10] C. Paus,[30] T.J. Phillips,[14] G. Piacentino[q],[15] E. Pianori,[40] J. Pilot,[7] K. Pitts,[22] C. Plager,[8] L. Pondrom,[53] S. Poprocki[f],[15] K. Potamianos,[26] A. Pranko,[26] F. Prokoshin[aa],[13] F. Ptohos[g],[17] G. Punzi[mm],[41] I. Redondo Fernández,[29] P. Renton,[38] M. Rescigno,[46] F. Rimondi,[6,*] L. Ristori,[41,15] A. Robson,[19] T. Rodriguez,[40] S. Rolli[h],[50] M. Ronzani[mm],[41] R. Roser,[15] J.L. Rosner,[11] F. Ruffini[nn],[41] A. Ruiz,[9] J. Russ,[10] V. Rusu,[15] W.K. Sakumoto,[44] Y. Sakurai,[51] L. Santi[sstt],[48] K. Sato,[49] V. Saveliev[v],[15] A. Savoy-Navarro[z],[15] P. Schlabach,[15] E.E. Schmidt,[15] T. Schwarz,[31] L. Scodellaro,[9] F. Scuri,[41] S. Seidel,[34] Y. Seiya,[37] A. Semenov,[13] F. Sforza[mm],[41] S.Z. Shalhout,[7] T. Shears,[27] P.F. Shepard,[42] M. Shimojima[u],[49] M. Shochet,[11] I. Shreyber-Tecker,[33] A. Simonenko,[13] K. Sliwa,[50] J.R. Smith,[7] F.D. Snider,[15] H. Song,[42] V. Sorin,[4] R. St. Denis,[19,*] M. Stancari,[15] D. Stentz[w],[15] J. Strologas,[34] Y. Sudo,[49] A. Sukhanov,[15] I. Suslov,[13] K. Takemasa,[49] Y. Takeuchi,[49] J. Tang,[11] M. Tecchio,[31] P.K. Teng,[1] J. Thom[f],[15] E. Thomson,[40] V. Thukral,[47] D. Toback,[47] S. Tokar,[12] K. Tollefson,[32] T. Tomura,[49] D. Tonelli[e],[15] S. Torre,[17] D. Torretta,[15] P. Totaro,[39] M. Trovato[oo],[41] F. Ukegawa,[49] S. Uozumi,[25] F. Vázquez[l],[16] G. Velev,[15] C. Vellidis,[15] C. Vernieri[oo],[41] M. Vidal,[43] R. Vilar,[9] J. Vizán[dd],[9] M. Vogel,[34] G. Volpi,[17] P. Wagner,[40] R. Wallny[j],[15] S.M. Wang,[1] D. Waters,[28] W.C. Wester III,[15] D. Whiteson[c],[40] A.B. Wicklund,[2] S. Wilbur,[7] H.H. Williams,[40] J.S. Wilson,[31] P. Wilson,[15]

B.L. Winer,[35] P. Wittich[f],[15] S. Wolbers,[15] H. Wolfe,[35] T. Wright,[31] X. Wu,[18] Z. Wu,[5] K. Yamamoto,[37] D. Yamato,[37] T. Yang,[15] U.K. Yang,[25] Y.C. Yang,[25] W.-M. Yao,[26] G.P. Yeh,[15] K. Yi[m],[15] J. Yoh,[15] K. Yorita,[51] T. Yoshida[k],[37] G.B. Yu,[14] I. Yu,[25] A.M. Zanetti,[48] Y. Zeng,[14] C. Zhou,[14] and S. Zucchelli[kk6]

(CDF Collaboration)[†]

[1] *Institute of Physics, Academia Sinica, Taipei, Taiwan 11529, Republic of China*
[2] *Argonne National Laboratory, Argonne, Illinois 60439, USA*
[3] *University of Athens, 157 71 Athens, Greece*
[4] *Institut de Fisica d'Altes Energies, ICREA, Universitat Autonoma de Barcelona, E-08193, Bellaterra (Barcelona), Spain*
[5] *Baylor University, Waco, Texas 76798, USA*
[6] *Istituto Nazionale di Fisica Nucleare Bologna, [kk] University of Bologna, I-40127 Bologna, Italy*
[7] *University of California, Davis, Davis, California 95616, USA*
[8] *University of California, Los Angeles, Los Angeles, California 90024, USA*
[9] *Instituto de Fisica de Cantabria, CSIC-University of Cantabria, 39005 Santander, Spain*
[10] *Carnegie Mellon University, Pittsburgh, Pennsylvania 15213, USA*
[11] *Enrico Fermi Institute, University of Chicago, Chicago, Illinois 60637, USA*
[12] *Comenius University, 842 48 Bratislava, Slovakia; Institute of Experimental Physics, 040 01 Kosice, Slovakia*
[13] *Joint Institute for Nuclear Research, RU-141980 Dubna, Russia*
[14] *Duke University, Durham, North Carolina 27708, USA*
[15] *Fermi National Accelerator Laboratory, Batavia, Illinois 60510, USA*
[16] *University of Florida, Gainesville, Florida 32611, USA*
[17] *Laboratori Nazionali di Frascati, Istituto Nazionale di Fisica Nucleare, I-00044 Frascati, Italy*
[18] *University of Geneva, CH-1211 Geneva 4, Switzerland*
[19] *Glasgow University, Glasgow G12 8QQ, United Kingdom*
[20] *Harvard University, Cambridge, Massachusetts 02138, USA*
[21] *Division of High Energy Physics, Department of Physics, University of Helsinki, FIN-00014, Helsinki, Finland; Helsinki Institute of Physics, FIN-00014, Helsinki, Finland*
[22] *University of Illinois, Urbana, Illinois 61801, USA*
[23] *The Johns Hopkins University, Baltimore, Maryland 21218, USA*
[24] *Institut für Experimentelle Kernphysik, Karlsruhe Institute of Technology, D-76131 Karlsruhe, Germany*
[25] *Center for High Energy Physics: Kyungpook National University, Daegu 702-701, Korea; Seoul National University, Seoul 151-742, Korea; Sungkyunkwan University, Suwon 440-746, Korea; Korea Institute of Science and Technology Information, Daejeon 305-806, Korea; Chonnam National University, Gwangju 500-757, Korea; Chonbuk National University, Jeonju 561-756, Korea; Ewha Womans University, Seoul, 120-750, Korea*
[26] *Ernest Orlando Lawrence Berkeley National Laboratory, Berkeley, California 94720, USA*
[27] *University of Liverpool, Liverpool L69 7ZE, United Kingdom*
[28] *University College London, London WC1E 6BT, United Kingdom*
[29] *Centro de Investigaciones Energeticas Medioambientales y Tecnologicas, E-28040 Madrid, Spain*
[30] *Massachusetts Institute of Technology, Cambridge, Massachusetts 02139, USA*
[31] *University of Michigan, Ann Arbor, Michigan 48109, USA*
[32] *Michigan State University, East Lansing, Michigan 48824, USA*
[33] *Institution for Theoretical and Experimental Physics, ITEP, Moscow 117259, Russia*
[34] *University of New Mexico, Albuquerque, New Mexico 87131, USA*
[35] *The Ohio State University, Columbus, Ohio 43210, USA*
[36] *Okayama University, Okayama 700-8530, Japan*
[37] *Osaka City University, Osaka 558-8585, Japan*
[38] *University of Oxford, Oxford OX1 3RH, United Kingdom*
[39] *Istituto Nazionale di Fisica Nucleare, Sezione di Padova, [ll] University of Padova, I-35131 Padova, Italy*
[40] *University of Pennsylvania, Philadelphia, Pennsylvania 19104, USA*
[41] *Istituto Nazionale di Fisica Nucleare Pisa, [mm] University of Pisa, [nn] University of Siena, [oo] Scuola Normale Superiore, I-56127 Pisa, Italy, [pp] INFN Pavia, I-27100 Pavia, Italy, [qq] University of Pavia, I-27100 Pavia, Italy*
[42] *University of Pittsburgh, Pittsburgh, Pennsylvania 15260, USA*
[43] *Purdue University, West Lafayette, Indiana 47907, USA*
[44] *University of Rochester, Rochester, New York 14627, USA*
[45] *The Rockefeller University, New York, New York 10065, USA*
[46] *Istituto Nazionale di Fisica Nucleare, Sezione di Roma 1, [rr] Sapienza Università di Roma, I-00185 Roma, Italy*
[47] *Mitchell Institute for Fundamental Physics and Astronomy, Texas A&M University, College Station, Texas 77843, USA*

[48] Istituto Nazionale di Fisica Nucleare Trieste, [ss] Gruppo Collegato di Udine,
[tt] University of Udine, I-33100 Udine, Italy, [uu] University of Trieste, I-34127 Trieste, Italy
[49] University of Tsukuba, Tsukuba, Ibaraki 305, Japan
[50] Tufts University, Medford, Massachusetts 02155, USA
[51] Waseda University, Tokyo 169, Japan
[52] Wayne State University, Detroit, Michigan 48201, USA
[53] University of Wisconsin-Madison, Madison, Wisconsin 53706, USA
[54] Yale University, New Haven, Connecticut 06520, USA
(Dated: February 27, 2017)

A measurement of the inclusive production cross section of isolated prompt photons in proton-antiproton collisions at center-of-mass energy $\sqrt{s} = 1.96$ TeV is presented. The results are obtained using the full Run II data sample collected with the Collider Detector at the Fermilab Tevatron, which corresponds to an integrated luminosity of 9.5 fb^{-1}. The cross section is measured as a function of photon transverse energy, E_T^γ, in the range $30 < E_T^\gamma < 500$ GeV and in the pseudorapidity region $|\eta^\gamma| < 1.0$. The results are compared with predictions from parton-shower Monte Carlo models at leading order in quantum chromodynamics (QCD) and from next-to-leading order perturbative QCD calculations. The latter show good agreement with the measured cross section.

PACS numbers: 12.38.Qk, 13.85.Qk

I. INTRODUCTION

The measurement of the cross section for the production of inclusive prompt photon (γ) in proton-antiproton ($p\bar{p}$) collisions is an important test for perturbative quantum chromodynamics (pQCD), probing the parton distribution functions (PDFs), and the parton-to-photon fragmentation functions (FFs) [1–3]. In addition, prompt-photon production is a major background for many other standard model (SM) processes such as Higgs-boson decays into photon pairs ($H \to \gamma\gamma$) and in searches for non-SM physics with final states containing photons [4–6].

The term "prompt" identifies photons that are produced directly in the hard interaction and do not arise from hadron decays. In $p\bar{p}$ collisions, events with prompt photons with transverse energy E_T^γ [7] smaller than approximately 100 GeV are produced predominantly via quark-gluon Compton scattering $qg \to q\gamma$, while at higher energies the quark-antiquark annihilation process $q\bar{q} \to g\gamma$ plays a dominant role. In addition, prompt photons are produced through the collinear fragmentation of a final-state parton into a photon, e.g., $qq \to qq \to \gamma X$, where X can be any set of final state particles.

The first measurement of the prompt-photon production cross section in hadron collisions came from the CERN Intersecting Storage Rings pp collider, followed by measurements at the $Sp\bar{p}S$ collider [8–11]. More recent prompt-photon measurements have been performed at the Fermilab Tevatron Collider by the CDF and D0 Collaborations using $p\bar{p}$ collisions collected at a center-of-mass energy $\sqrt{s} = 1.8$ TeV and 1.96 TeV [12–14] and at the CERN Large Hadron Collider by the ATLAS and CMS Collaborations using pp collisions at $\sqrt{s} = 7$ TeV [15–19], 8 TeV [20], and 13 TeV [21].

This article presents a measurement of the inclusive cross section for isolated prompt photons over the range $30 < E_T^\gamma < 500$ GeV, based on the full data set collected by the Collider Detector (CDF) during Run II (2001–2011) of the Fermilab Tevatron collider and corresponding to an integrated luminosity of 9.5 fb^{-1} [22].

---

* Deceased

† With visitors from [a] University of British Columbia, Vancouver, BC V6T 1Z1, Canada, [b] Istituto Nazionale di Fisica Nucleare, Sezione di Cagliari, 09042 Monserrato (Cagliari), Italy, [c] University of California Irvine, Irvine, CA 92697, USA, [d] Institute of Physics, Academy of Sciences of the Czech Republic, 182 21, Czech Republic, [e] CERN, CH-1211 Geneva, Switzerland, [f] Cornell University, Ithaca, NY 14853, USA, [g] University of Cyprus, Nicosia CY-1678, Cyprus, [h] Office of Science, U.S. Department of Energy, Washington, DC 20585, USA, [i] University College Dublin, Dublin 4, Ireland, [j] ETH, 8092 Zürich, Switzerland, [k] University of Fukui, Fukui City, Fukui Prefecture, Japan 910-0017, [l] Universidad Iberoamericana, Lomas de Santa Fe, México, C.P. 01219, Distrito Federal, [m] University of Iowa, Iowa City, IA 52242, USA, [n] Kinki University, Higashi-Osaka City, Japan 577-8502, [o] Kansas State University, Manhattan, KS 66506, USA, [p] Brookhaven National Laboratory, Upton, NY 11973, USA, [q] Istituto Nazionale di Fisica Nucleare, Sezione di Lecce, Via Arnesano, I-73100 Lecce, Italy, [r] Queen Mary, University of London, London, E1 4NS, United Kingdom, [s] University of Melbourne, Victoria 3010, Australia, [t] Muons, Inc., Batavia, IL 60510, USA, [u] Nagasaki Institute of Applied Science, Nagasaki 851-0193, Japan, [v] National Research Nuclear University, Moscow 115409, Russia, [w] Northwestern University, Evanston, IL 60208, USA, [x] University of Notre Dame, Notre Dame, IN 46556, USA, [y] Universidad de Oviedo, E-33007 Oviedo, Spain, [z] CNRS-IN2P3, Paris, F-75205 France, [aa] Universidad Tecnica Federico Santa Maria, 110v Valparaiso, Chile, [bb] Sejong University, Seoul 143-747, Korea, [cc] The University of Jordan, Amman 11942, Jordan, [dd] Universite catholique de Louvain, 1348 Louvain-La-Neuve, Belgium, [ee] University of Zürich, 8006 Zürich, Switzerland, [ff] Massachusetts General Hospital, Boston, MA 02114 USA, [gg] Harvard Medical School, Boston, MA 02114 USA, [hh] Hampton University, Hampton, VA 23668, USA, [ii] Los Alamos National Laboratory, Los Alamos, NM 87544, USA, [jj] Università degli Studi di Napoli Federico II, I-80138 Napoli, Italy

II. THE CDF II DETECTOR

The CDF II detector [23] is a general-purpose spectrometer at the Fermilab Tevatron collider. It has a cylindrical geometry with approximate forward-backward and azimuthal symmetry. It includes a charged-particle tracking system consisting of silicon microstrip detectors and a cylindrical open-cell drift chamber, designed to measure charged-particle trajectories (tracks) and momenta. The tracking system is contained within a 1.4 T axial magnetic field. It is surrounded by electromagnetic (EM) and hadronic calorimeters segmented in projective towers and used to identify and measure the energy and position of photons, electrons, hadrons, and clusters of particles (jets). The central calorimeters cover the region $|\eta| < 1.1$, and have electromagnetic transverse-energy resolution of $\sigma(E_T)/E_T = 13.5\%/\sqrt{E_T(\mathrm{GeV})} \oplus 1.5\%$ and a tower segmentation of $\Delta\eta \times \Delta\phi \approx 0.1\times15^\circ$ in pseudorapidity-angular space [7]. At a depth corresponding approximately to the maximum energy density in the development of a typical EM shower, the EM calorimeters contain detectors that measure the transverse shower profile. The electromagnetic compartments of the calorimeter are equipped with a timing system measuring the arrival time of particles that deposit energy in each tower [24]. Drift chambers and scintillation counters located outside the calorimeters identify muons.

III. DATA AND SIMULATED SAMPLES

A. Event selection

Photons are reconstructed using clusters of (up to three) adjacent towers above threshold in the central EM calorimeter [25]. The pseudorapidity is restricted to the fiducial region $|\eta^\gamma| < 1.0$. The data are collected using a three-level online event-filtering system (trigger) [26] that selects events with at least one EM cluster consistent with a photon in the final state. Since there can be multiple collisions in the same bunch crossing, the event primary vertex ($p\bar{p}$ interaction point) is chosen to be the one that results in the best balance of the p_T of the photon; the z position of the reconstructed primary vertex is required to be within 60 cm of the center of the detector. The photon transverse energy is corrected to account for nonuniformities in the calorimeter response, and calibrated using electrons from reconstructed Z-boson decays [27]. Photon candidates are required to satisfy $E_T^\gamma > 30$ GeV and to meet requirements on calorimeter isolation [28], on track isolation [28], and on the ratio of the energy deposited in the hadronic calorimeter to the energy in the EM cluster [25]. If more than one prompt photon candidate is reconstructed ($\approx 1\%$ of the photon events), that with the highest E_T (leading photon) is chosen.

Events with electrons from Z- and W-boson decays, which can be misidentified as photons, are removed from the sample by requiring 0 tracks, or at the most one soft track (track isolation $\leq$5 GeV), pointing to the EM cluster. This track is allowed to account for underlying event and pile-up energy around the cluster. The number of electrons coming from W-boson decays is further reduced by requiring the missing transverse energy [7] of the event to be less than 80% of the transverse energy of the photon candidate. This requirement also reduces backgrounds arising from other sources that lead to energy imbalance, such as muons from cosmic rays that may emit bremsstrahlung radiation in the calorimeter, and muons from beam-halo interactions with the beam pipe, which may in turn interact with the detector material producing photons. Finally, the EM signal timing is required to be consistent with the $p\bar{p}$ collision time [25]. The residual backgrounds from Z- and W-boson decays, cosmic rays and beam halo, are expected to be less than 1% of the total sample.

After applying all the selection criteria, 2.1×10^6 events remain in the $\gamma + X$ data sample. The dominant remaining backgrounds are due to jets misidentified as photons.

B. Simulated events

Simulated events from the PYTHIA Monte-Carlo (MC) generator [29] are used in the background estimation, and to evaluate the product of the detector acceptance (A) and the efficiency (ϵ) for signal events. Monte Carlo samples are generated with PYTHIA 6.216, a parton-shower generator at leading-order (LO) in the strong-interaction coupling, with the CTEQ5L PDFs [29]. The PYTHIA predictions include $2 \to 2$ matrix-element subprocesses. Higher-order QCD corrections are included by initial- and final-state parton showers.

For the study of systematic uncertainties and for comparisons with the final results, events are also generated with the SHERPA 1.4.1 MC generator [30] with CT10 PDFs [31]. The SHERPA predictions include all the tree-level matrix-element amplitudes with one photon and up to three partons. This calculation features a parton-jet matching procedure to avoid an overlap between the phase-space descriptions given by the fixed-order matrix-element subprocesses and the showering and hadronization in the multijet simulation.

The TUNE A [32, 33] underlying event [34] model is used in the PYTHIA calculation. Monte Carlo events are passed through a GEANT-based simulation of the detector [35] and subjected to the same reconstruction and selection requirements as the data.

IV. SIGNAL FRACTION

After the event selection, the remaining background comes from the decays of hadrons (such as $\pi^0 \to \gamma\gamma$); they cannot be rejected on an event-by-event basis, so a statistical background-subtraction technique is used to measure the signal cross section. To evaluate the sig-

nal fraction, an artificial neural network (ANN) is defined using as input the shower-shape, transverse profile, and isolation variables [36]. The inclusive-photon simulation is matched to data by applying the same corrections as derived in Refs. [13, 37]. Further, MC events are reweighted to the observed instantaneous luminosity profile to account for luminosity-dependent effects. The expected ANN output distributions ("templates") for signal and background samples are constructed using PYTHIA inclusive-photon and dijet MC predictions, respectively. These templates are validated using the $Z \to e^+e^-$ and dijet data samples [37]. To estimate the prompt-photon rate, the ANN output distribution observed in data is fit to a linear combination of signal and background ANN templates, using a binned maximum-likelihood method that accounts for uncertainties on both data and templates [38]. A fit is performed in each E_T^γ bin, yielding prompt-photon fractions in the E_T^γ range from 30 GeV up to 500 GeV, as shown in Fig. 1 for an example E_T^γ bin. Figure 2 shows the resulting signal fraction (photon purity) as a function of E_T^γ.

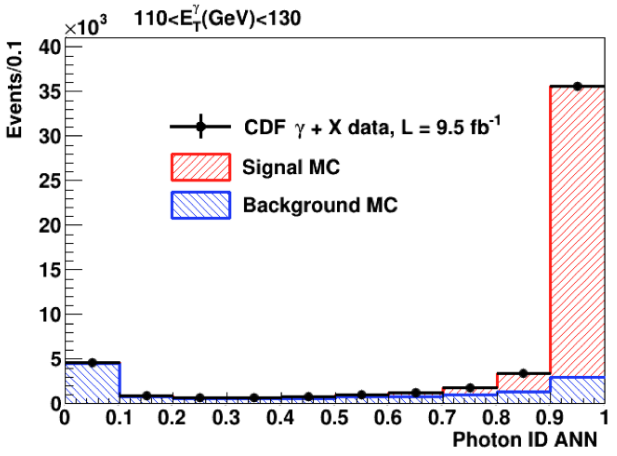

FIG. 1. Observed ANN output distribution (points), the templates for signal and background processes, and the resulting fit of the templates to the data distribution, for events restricted to the photon transverse energy bin 110–130 GeV. The left-hatched histogram (blue in color) represents the background and the right-hatched histogram (red in color) represents the signal, normalized so that the scale of the sum of the templates equals the total number of data events.

The systematic uncertainty on the signal fraction is estimated by varying the fit configurations and the values of the ANN input variables within their uncertainties. The dominant uncertainty on the shape of the ANN templates originates from the modeling of calorimeter isolation energy. The overall systematic uncertainty on the signal fraction is estimated to be 8% at low E_T^γ, 6% at high E_T^γ, and 3% on average for the intermediate E_T^γ range $40 < E_T^\gamma < 300$ GeV.

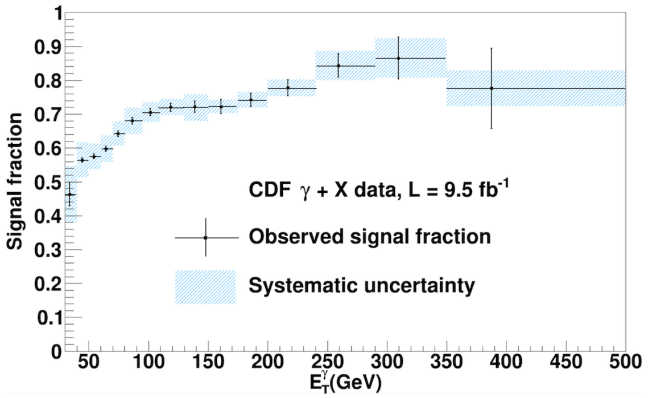

FIG. 2. Signal fraction as a function of leading-photon E_T. The points are plotted at the average E_T^γ, of the data within each bin. The error bars represent the statistical uncertainty, while bands represent the total systematic uncertainty.

V. CROSS SECTION MEASUREMENT

The differential cross section for the production of isolated prompt photons in a given phase-space bin is calculated as $d^2\sigma/(dE_T^\gamma d\eta^\gamma) = (Nf^\gamma)/(\Delta E_T^\gamma \Delta\eta^\gamma \mathcal{L} A \times \epsilon)$, where N is the number of data events in a given E_T^γ bin after applying the full selection, f^γ is the signal fraction, ΔE_T^γ is the width of the E_T^γ bin, $\mathcal{L}$ is the integrated luminosity, and $A \times \epsilon$ is a correction factor. Since the cross section is measured for $|\eta^\gamma| < 1.0$, $\Delta\eta^\gamma$ is set to 2.0.
The factor $A \times \epsilon$ combines corrections for acceptance, resolution effects and efficiencies for selecting and reconstructing the photon to infer the results at the particle level (*i.e.*, generator level). The correction is computed from the bin-by-bin fraction of simulated particle-level prompt photons in the reconstructed signal events, as determined by the PYTHIA MC calculation. The numerator is obtained by applying the same requirements to the PYTHIA-simulated events as those applied to data. The denominator is obtained by selecting generated particles [39] in the fiducial region, with $E_T^\gamma > 30$ GeV and the same energy isolation requirement as in the data. The photon efficiency is calibrated by comparing the selection efficiencies for $Z \to e^+e^-$ events in data and in simulation [37].

The largest sources of systematic uncertainty arise from the photon energy scale at high E_T ($\approx 6\%$) and from the $A \times \epsilon$ factor ($\approx 8\%$). The latter is determined by a comparison of results from the PYTHIA and SHERPA MC calculations.

VI. THEORETICAL PREDICTIONS

The predicted prompt-photon production cross section is calculated using the fixed-order next-to-leading-order (NLO) program MCFM 6.8 including nonperturba-

tive fragmentation at LO [40]. The calculation uses the MRST2008 NLO PDFs and the GdRG LO FFs [41]. The MCFM prediction is a parton-level calculation that does not include a model for the underlying event energy. This prediction is corrected for the nonperturbative effects of parton-to-hadron fragmentation and for underlying event energy. A correction factor $C_{\rm UE} = 0.91 \pm 0.03$ is defined as the overall ratio of the cross section obtained using the PYTHIA MC generator, with and without modeling of both multiple-parton interactions and hadronization [13].

The nominal renormalization (μ_R), factorization (μ_F), and fragmentation (μ_f) scales are set to the photon transverse energy ($\mu_R = \mu_F = \mu_f = E_T^\gamma$). The scale uncertainty is evaluated by varying the three scales simultaneously between the extreme values $E_T^\gamma/2$ and $2E_T^\gamma$.

In addition to comparison with the perturbative-QCD prediction above, we also compare the measured cross section to predictions from the PYTHIA and SHERPA MC generators. Both are calculated at the particle level, meaning that the photon isolation energy is estimated using generated hadrons and the selection criteria are applied to the hadron jets and are directly comparable to our measurement.

VII. RESULTS

The differential cross section results for the production of isolated prompt photons are listed in Table I, together with statistical and systematic uncertainties. The systematic uncertainties on the differential cross section are determined by propagating the sources of uncertainty considered for f^γ and $A \times \epsilon$. At low E_T^γ the total systematic uncertainty is dominated by the uncertainties in the ANN-template modeling, while the dependence of the $A \times \epsilon$ factors on the event generator gives the dominant contribution ($\approx 10\%$) to the uncertainty at intermediate and high E_T^γ. Finally, there is an additional 6% uncertainty on the integrated luminosity [42].

TABLE I. Measured cross section for the production of prompt isolated photons within the pseudorapidity region $|\eta^\gamma| < 1.0$, in bins of E_T^γ. $\langle E_T^\gamma \rangle$, the average E_T^γ within each bin, is listed for illustration of the steeply falling spectral shape. The measured-cross-section uncertainties given are statistical only. The column $\delta\sigma_{syst}$ gives the systematic uncertainties. The additional 6% luminosity uncertainty is not included in the table.

E_T^γ (GeV)	$\langle E_T^\gamma \rangle$ (GeV)	$d^2\sigma/(dE_T^\gamma d\eta^\gamma)$ (pb/GeV)	$\delta\sigma_{\rm syst}$ (%)
30–40	34.1	$(5.49 \pm 0.41)\times10^{1}$	23.3
40–50	44.3	$(1.72 \pm 0.23)\times10^{1}$	17.2
50–60	54.3	$(6.72 \pm 0.11)\times10^{0}$	14.9
60–70	64.4	$(2.95 \pm 0.04)\times10^{0}$	14.6
70–80	74.5	$(1.45 \pm 0.02)\times10^{0}$	13.7
80–90	86.5	$(6.87 \pm 0.10)\times10^{-1}$	13.2
90–110	101.7	$(3.03 \pm 0.05)\times10^{-1}$	12.8
110–130	118.7	$(1.32 \pm 0.03)\times10^{-1}$	12.7
130–150	138.8	$(5.65 \pm 0.15)\times10^{-2}$	13.1
150–175	160.9	$(2.37 \pm 0.08)\times10^{-2}$	12.6
175–200	185.9	$(1.03 \pm 0.03)\times10^{-2}$	12.4
200–240	216.8	$(4.01 \pm 0.12)\times10^{-3}$	13.2
240–290	259.2	$(1.16 \pm 0.05)\times10^{-3}$	14.1
290–350	309.4	$(3.08 \pm 0.23)\times10^{-4}$	15.1
350–500	387.6	$(1.83 \pm 0.29)\times10^{-5}$	16.1

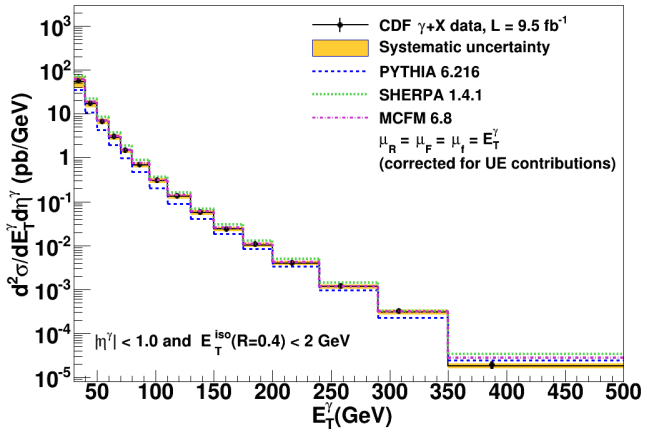

FIG. 3. Measured $\gamma + X$ cross section as a function of leading photon transverse energy. Data (markers) are centered at the average E_T^γ of each bin for illustration of the steeply falling spectral shape. Data are compared with the PYTHIA, SHERPA and MCFM predictions (dashed lines). The vertical error bars show the statistical uncertainties, while the shaded areas show the systematic uncertainties. The 6% luminosity uncertainty on the data is not included. A correction $C_{\rm UE}$ to account for parton-to-hadron fragmentation and underlying event effects is applied to the MCFM theoretical predictions, as explained in the text.

These results are compared with the theoretical predictions in Fig. 3. The ratio of the measured cross section over the predicted ones is shown in Fig. 4. The full error bars on the data points represent statistical and systematic uncertainties summed in quadrature. The inner error bars show statistical uncertainties only. The NLO predictions are shown with their theoretical uncertainties arising from the choice of factorization, renormalization, and fragmentation scales.

The NLO calculations agree with the data up to the highest E_T^γ-values considered. Observed cross sections are moderately larger than the central values for the NLO calculation for low E_T^γ, but agree within the theoretical uncertainty of the NLO calculation.

The PYTHIA and SHERPA predictions are also shown in Figs. 3 and 4. The shape of the measured-cross-section distribution is well described by both models. The PYTHIA prediction underestimates the observed cross section by more than a factor of 1.5 across the whole E_T^γ range. This is possibly due to the lack of higher-order terms in the PYTHIA photon+jet matrix-elements. The SHERPA calculation is approximately 1.1 to 1.2 times larger than the observed cross section, nearly uniformly

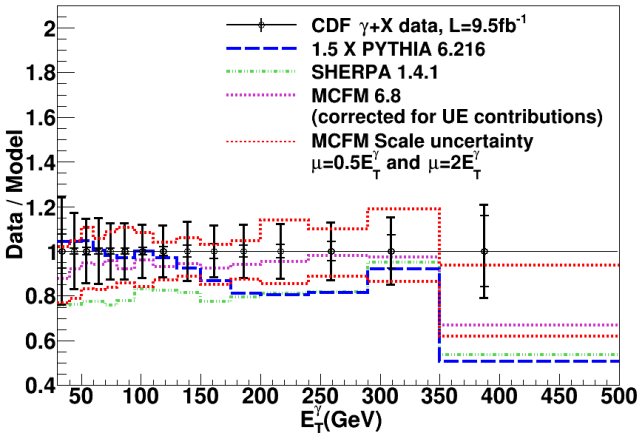

FIG. 4. Data points centered at 1.0 and data-to-theory ratio (dashed lines) of the inclusive prompt-photon differential cross section as a function of the photon transverse energy, in the pseudorapidity region $|\eta^\gamma| < 1.0$. The inner error bars on the data points show statistical uncertainties. The full error bars show statistical and systematic uncertainties added in quadrature. The 6% luminosity uncertainty on the data is not included. The LO PYTHIA prediction is multiplied by a factor 1.5.

across the E_T^γ range. This calculation includes up to three jet emissions associated with the observed photon, but it is missing virtual corrections in the matrix elements of the subprocesses, which could possibly explain the discrepancy with data. Other possible reasons are related to nonperturbative QCD processes, such as mistuned fragmentation subprocesses leading to excessive rates of photon production through fragmentation.

VIII. CONCLUSIONS

A measurement of the differential cross section for the inclusive production of isolated prompt photons in $p\bar{p}$ collisions at $\sqrt{s} = 1.96$ TeV is presented using the full data set collected with the CDF II detector at the Tevatron. The cross section is measured as a function of photon transverse energy E_T^γ in the central pseudorapidity region $|\eta^\gamma| < 1.0$. The measurement spans the E_T^γ kinematic range from 30 GeV to 500 GeV, thus extending the reach by 100 GeV from the previous CDF measurement [13]. Comparisons of our measurement to three theoretical predictions are discussed. Both PYTHIA and SHERPA predictions correctly describe the shape of the differential cross section. The PYTHIA generator predicts a smaller cross section compared to the data and the SHERPA prediction. The data are in good agreement with the fixed-order NLO MCFM calculation.

ACKNOWLEDGEMENTS

We thank the Fermilab staff and the technical staffs of the participating institutions for their vital contributions. This work was supported by the U.S. Department of Energy and National Science Foundation; the Italian Istituto Nazionale di Fisica Nucleare; the Ministry of Education, Culture, Sports, Science and Technology of Japan; the Natural Sciences and Engineering Research Council of Canada; the National Science Council of the Republic of China; the Swiss National Science Foundation; the A.P. Sloan Foundation; the Bundesministerium für Bildung und Forschung, Germany; the Korean World Class University Program, the National Research Foundation of Korea; the Science and Technology Facilities Council and the Royal Society, United Kingdom; the Russian Foundation for Basic Research; the Ministerio de Ciencia e Innovación, and Programa Consolider-Ingenio 2010, Spain; the Slovak R&D Agency; the Academy of Finland; the Australian Research Council (ARC); and the EU community Marie Curie Fellowship Contract No. 302103.

[1] J. F. Owens, Rev. Mod. Phys. **59**, 465 (1987).
[2] W. Vogelsang and A. Vogt, Nucl. Phys. **B453**, 334 (1995).
[3] L. Bourhis, M. Fontannaz, and J. Guillet, Eur. Phys. J. C **2**, 529 (1998).
[4] T. Binoth, in *QCD and high energy hadronic interactions. Proceedings, 35th Rencontres de Moriond, Les Arcs, France, March 18-25, 2000* (2000) pp. 151–154, arXiv:hep-ph/0005194.
[5] L. Randall and R. Sundrum, Phys. Rev. Lett. **83**, 3370 (1999).
[6] M. Dine, W. Fischler, and M. Srednicki, Nucl. Phys. **B189**, 575 (1981).
[7] A cylindrical coordinate system (r, ϕ, z) is used with origin at the geometric center of the detector; r is the radius from the nominal beam line, ϕ is the azimuthal angle, and the $+z$ axis points along the incident proton beam direction. The polar angle θ with respect to the proton beam is used to define the pseudorapidity $\eta = -\ln(\tan(\theta/2))$. Transverse energy and transverse momentum are defined as $E_T = E\sin(\theta)$ and $p_T = p\sin(\theta)$, respectively. The missing transverse energy is given by $\vec{\not\!\!E}_{\rm T} = -\sum_i E_T^i \hat{n}_i$ where i is the calorimeter tower number and $\hat{n}_i$ is a unit vector perpendicular to the beam axis and pointing at the ith calorimeter tower.
[8] E. Anassontzis *et al.* (R806 Collaboration), Z. Phys. C **13**, 277 (1982).
[9] A. Angelis *et al.* (CMOR Collaboration), Nucl. Phys. **B327**, 541 (1989).

[10] C. Albajar *et al.* (UA1 Collaboration), Phys. Lett. B **209**, 385 (1988).

[11] M. Werlen *et al.* (UA6 Collaboration), Phys. Lett. B **452**, 201 (1999).

[12] D. Acosta *et al.* (CDF Collaboration), Phys. Rev. D **65**, 112003 (2002).

[13] T. Aaltonen *et al.* (CDF Collaboration), Phys. Rev. D **80**, 111106 (2009).

[14] V. Abazov *et al.* (D0 Collaboration), Phys. Lett. B **639**, 151 (2006).

[15] G. Aad *et al.* (ATLAS Collaboration), Phys. Rev. D **83**, 052005 (2011).

[16] G. Aad *et al.* (ATLAS Collaboration), Phys. Lett. B **706**, 150 (2011).

[17] G. Aad *et al.* (ATLAS Collaboration), Phys. Rev. D **89**, 052004 (2014).

[18] V. Khachatryan *et al.* (CMS Collaboration), Phys. Rev. Lett. **106**, 082001 (2011).

[19] S. Chatrchyan *et al.* (CMS Collaboration), Phys. Rev. D **84**, 052011 (2011).

[20] G. Aad *et al.* (ATLAS Collaboration), J. High Energy Phys. 08 (2016) 005.

[21] M. Aaboud *et al.* (ATLAS Collaboration), submitted to Phys. Lett. B, arXiv:hep-ex/1701.06882v1.

[22] The data set for this measurement corresponds to an integrated luminosity four times larger than that of the previously published CDF measurement [13].

[23] R. Blair *et al.* (CDF Collaboration), FERMILAB-DESIGN-1996-01, FERMILAB-PUB-96-390-E (1996).

[24] M. Goncharov *et al.*, Nucl. Instrum. Methods Phys. Res., Sect. A **565**, 543 (2006).

[25] T. Aaltonen *et al.* (CDF Collaboration), Phys. Rev. D **82**, 052005 (2010).

[26] F. Abe *et al.* (CDF Collaboration), Nucl. Instrum. Methods Phys. Res., Sect. A **271**, 387 (1988).

[27] T. Aaltonen *et al.* (CDF Collaboration), Phys. Rev. Lett. **103**, 061803 (2009).

[28] The calorimeter isolation is defined as the transverse energy deposits in the EM calorimeter in the isolation cone minus the transverse energy in the EM cluster of the photon. The isolation cone is defined to have a radius $R = \sqrt{(\Delta\eta)^2 + (\Delta\phi)^2} = 0.4$. The track isolation is defined as the scalar sum of the transverse momenta of all tracks originating from the primary vertex of the event and lying within a cone of radius $R = 0.4$.

[29] T. Sjöstrand, S. Mrenna, and P. Skands, J. High Energy Phys. 05 (2006) 026.

[30] T. Gleisberg, S. Hoeche, F. Krauss, M. Schonherr, S. Schumann, F. Siegert, and J. Winter, J. High Energy Phys. 02 (2009) 007.

[31] S. Höeche, S. Schumann, and F. Siegert, Phys. Rev. D **81**, 034026 (2010).

[32] R. Field and R. C. Group (CDF Collaboration), CDF-ANAL-CDF-PUBLIC-7822 (2005), arXiv:hep-ph/0510198.

[33] T. Affolder *et al.* (CDF Collaboration), Phys. Rev. D **65**, 092002 (2002).

[34] The underlying event is that part of the event final state that cannot be directly associated with the primary hard 2→2 parton-parton scattering and consists of the beam remnants plus possible contributions from initial- and final-state gluon radiation and additional parton-parton interactions.

[35] R. Brun and F. Carminati, CERN Programming Library Long Writeup **W5013** (1993).

[36] T. Aaltonen *et al.* (CDF Collaboration), Phys. Rev. Lett. **108**, 011801 (2012).

[37] T. Aaltonen *et al.* (CDF Collaboration), Phys. Rev. Lett. **111**, 042003 (2013).

[38] As implemented in TFractionFitter which is a class of the CERN Root analysis software [43, 44]. The fit fractions are provided with an error estimate which takes into account both data and Monte Carlo statistical uncertainties. TFractionFitter errors are corrected based on pseudoexperiments [45].

[39] Generated particles are the stable particles, i.e., particles with a lifetime of at least 10 ps in events from MC generators, without any simulation of the interaction of these particles with the detector or any additional proton-antiproton interactions.

[40] J. Campbell and R. Ellis, Phys. Rev. D **65**, 113007 (2002).

[41] A. Gehrmann-De Ridder and E. W. N. Glover, Eur. Phys. J. C **7**, 29 (1999).

[42] A. Abulencia *et al.* (CDF), J. Phys. **G34**, 2457 (2007), arXiv:hep-ex/0508029 [hep-ex].

[43] R. Brun and F. Rademakers, *New computing techniques in physics research V. Proceedings, 5th International Workshop, AIHENP '96, Lausanne, Switzerland, September 2-6, 1996*, Nucl. Instrum. Methods Phys. Res., Sect. A **389**, 81 (1997), see also `http://root.cern.ch/`.

[44] R. Barlow and C. Beeston, Comp. Phys. Comm. **77**, 219 (1993).

[45] A. Lucà, Ph.D. thesis, University of Rome Tor Vergata, [FERMILAB-THESIS-2016-08, 2016].